Double transition-metal MXenes: Atomistic design of two-dimensional carbides and nitrides

Weichen Hong†, Brian C. Wyatt†, Srinivasa Kartik Nemani†, and Babak Anasori

MXenes are a large family of two-dimensional (2D) transition-metal carbides, nitrides, and carbonitrides. The MXene family has expanded since their original discovery in 2011, and has grown larger with the discovery of ordered double transition-metal (DTM) MXenes. These DTM MXenes differ from their counterpart mono-transition-metal (mono-M) MXenes, where two transition metals can occupy the metal sites. Ordered DTM MXenes are comprised of transition metals in either an in-plane or out-of-plane ordered structure. Additionally, some DTM MXenes are in the form of random solid solutions, which are defined by two randomly distributed transition metals throughout the 2D structure. Their different structures and array of transition-metal pairs provide the ability to tune DTM MXenes for specific optical, magnetic, electrochemical, thermoelectric, catalytic, or mechanical behavior. This degree of control over their composition and structure is unique in the field of 2D materials and offers a new avenue for application-driven design of functional nanomaterials. In this article, we review the synthesis, structure, and properties of DTM MXenes and provide an outlook for future research in this field. (†: Authors contributed equally.)

Introduction

There has been significant interest in the design of two-dimensional (2D) materials since the characterization of single layer graphene in 2004[1] to meet rapidly evolving demands for advanced materials in technological applications, including energy storage,[2-4] electronics,[5] membranes,[6,7] catalysts,[8] and sensors.[9,10] MXenes are a large family of 2D materials, discovered in 2011,[11,12] which offer a unique combination of electronic,[13-15] optical,[16-18] mechanical,[19-21] and colloidal properties.[22,23] MXenes are few-atoms-thick 2D sheets with a general formula of $M_{n+1}X_nT_x$. In each MXene flake, $n + 1$ (n = 1–4) layers of a transition metal (M) are interleaved with n layers of carbon or nitrogen (X).[24,25] The T_x in the formula represents surface terminations, including =O, –OH, –F, and –Cl, which are bonded to the outer M layers.[24,26,27] MXenes have high metallic conductivity (up to 15,100 S·cm^{-1} in $Ti_3C_2T_x$ film form),[28] are optically transparent (absorbing 3% of visible light/nm thickness),[18] exhibit a high modulus of elasticity (330–400 GPa),[19-21] and can act as electromagnetic interference shields[29] and electrochemically active materials.[24]

MXenes synthesis is a top-down approach, by selectively etching the A-layers from three-dimensional (3D) crystalline layered carbides and nitrides,[30,31] mostly MAX phases. In a MAX phase, $M_{n+1}X_n$ layers are bonded with an atomic layer of an A-group element, which is usually a group 13 to 16 element (Al, Ga, Si, Ge, P, and As).[32] Three types of MAX phase structures, M_2AX, M_3AX_2, and M_4AX_3, are shown in **Figure 1**a.

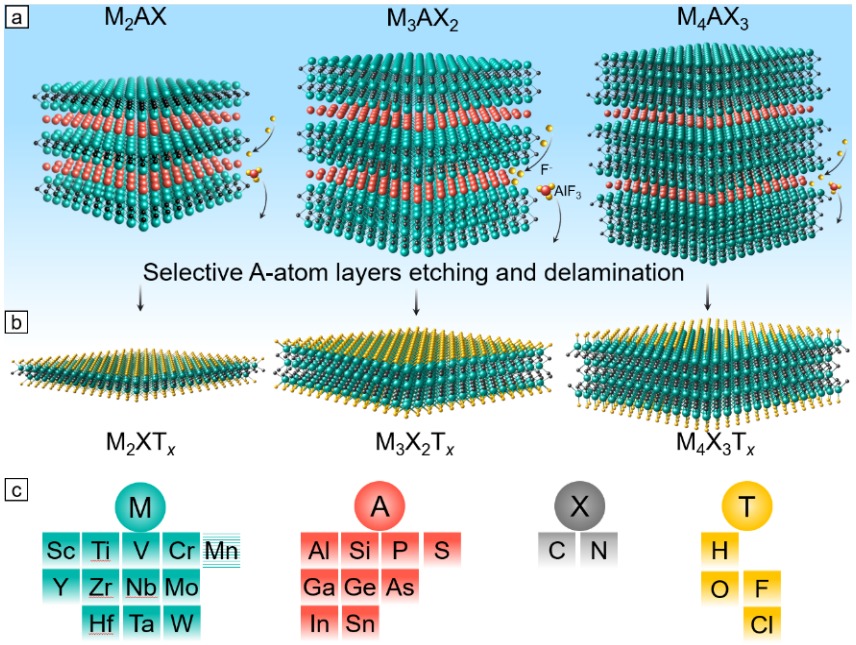

Figure 1. MXenes precursors and their synthesis. (a) Three types of mono-M MAX phases M_2AX, M_3AX_2, M_4AX_3 and the selective etching process of the A-group layers (red atoms). (b) MXenes are formed after selective etching and formation of surface terminations (yellow atoms) labeled as T. (c) Possible elements for M, A, X, and T in MAX and MXene phases. Additionally, MXene orders as high as M_5X_4 has been synthesized, but not included in this table. Mn exists in M sites in MAX phases, but Mn-containing MXenes have not yet been synthesized, as denoted by the horizontal patterned background of Mn.

Weichen Hong, Department of Mechanical and Energy Engineering and Integrated Nanosystems Development Institute, Purdue School of Engineering and Technology, Indiana University–Purdue University Indianapolis , USA ; hweichen@purdue.edu
Brian C. Wyatt, Department of Mechanical and Energy Engineering and Integrated Nanosystems Development Institute, Purdue School of Engineering and Technology, Indiana University–Purdue University Indianapolis , USA ; bcwyatt@iu.edu
Srinivasa Kartik Nemani, Department of Mechanical and Energy Engineering and Integrated Nanosystems Development Institute, Purdue School of Engineering and Technology, Indiana University–Purdue University Indianapolis , USA ; snemani@iu.edu
Babak Anasori, Department of Mechanical and Energy Engineering and Integrated Nanosystems Development Institute, Purdue School of Engineering and Technology, Indiana University–Purdue University Indianapolis, USA ; banasori@iupui.edu

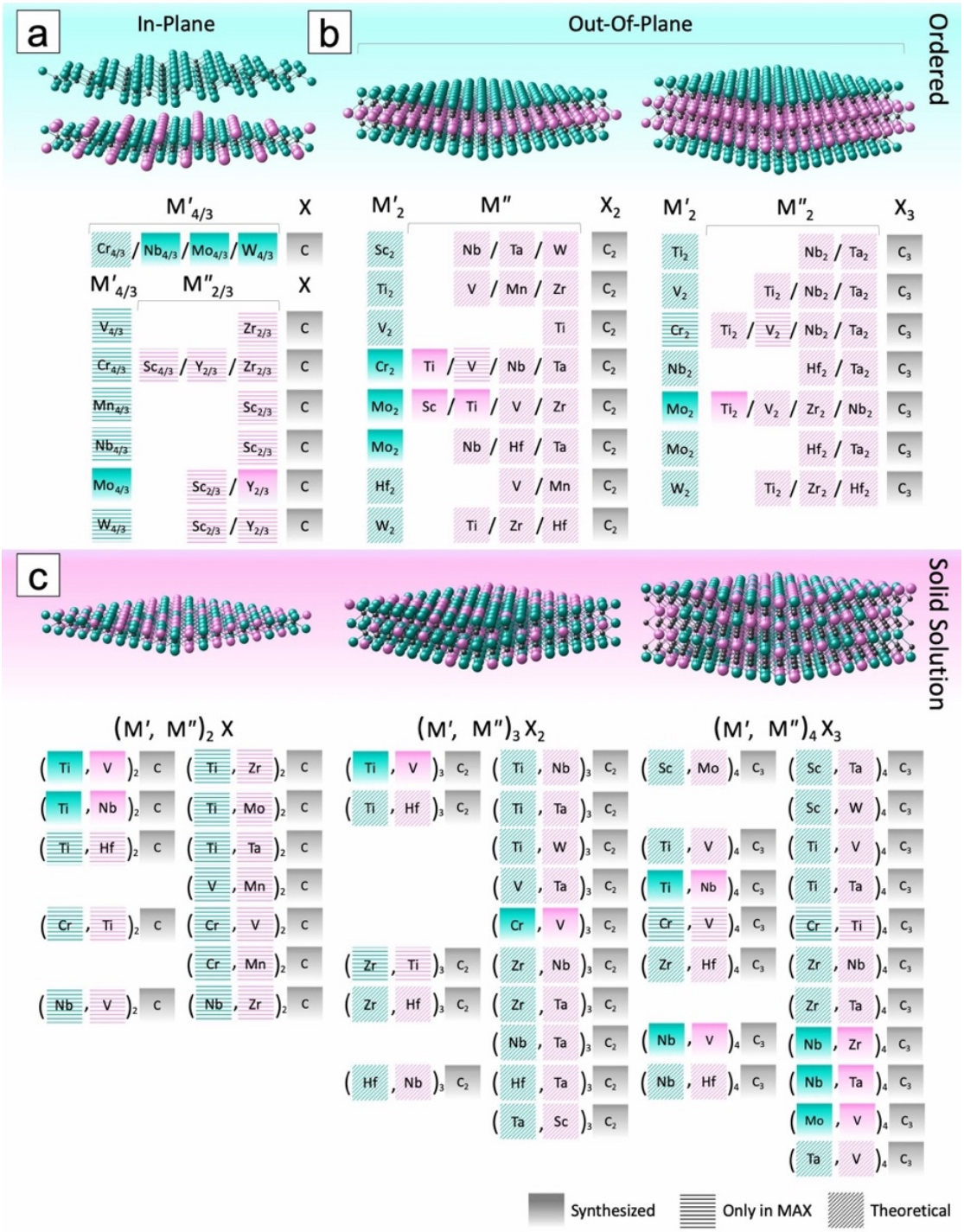

Figure 2. Experimentally synthesized and theoretical double transition-metal (DTM) M_2X, M_3X_2, and M_4X_3 MXenes. The green and purple elements correspond to M′ and M″ transition metals, respectively. (a) In-plane order ($M'_{4/3}M''_{2/3}X$ shown below) and in-plane divacancy order ($M'_{4/3}X$ shown above). (b) Out-of-plane order ($M'_2M''X_2$ and $M'_2M''_2X_3$). (c) Solid-solution MXenes are disordered, with M′ and M″ transition metals occupying random sites. In addition, solid solution $(Mo_{0.8}V_{0.2})_5C_4T_x$ has been successfully synthesized, but has not been displayed for simplicity. M elements with solid gradient background refer to experimentally synthesized MXenes, while M elements with diagonal striped background represent MXenes explored by first-principles studies, but are yet to be synthesized. M elements with horizontal stripes represent experimentally realized MAX phase precursors, but have not been etched to MXenes. In this figure, surface terminations (T_x: =O,–OH,–F, and–Cl) are not shown for simplicity.

MAX phases are usually synthesized by reactive sintering of their elemental powder in stoichiometric ratios, such as 3M:1A:2C for M_3AC_2, at temperatures above 1300ºC under controlled atmosphere.[32] The M–A bonds are primary bonds, which makes mechanical exfoliation challenging. However, the M–A bonds are weaker in comparison to M–X bonds, which allows selective chemical etching of the A elements without disruption of the M–X bonds.[33] This consequently permits $M_{n+1}X_n$ layers to be readily delaminated.[11,33] After selective removal of the A-group layers, transition metals in $M_{n+1}X_n$ are exposed. After exposure, M-elements become terminated with surface functional groups (T_x), which forms the chemical formula $M_{n+1}X_nT_x$ (Figure 1b). The composition of surface terminations is determined by the chemistry of the environment during etching and posttreatment methods,[34-38] as well as the nature of the M transition metal.[34] The list of elements for M, X, T, and some of the A-group elements of MAX phases are shown in Figure 1c. The full list of A-group elements of MAX phases can be found elsewhere.[27,32] Recently, a thicker family of MXene with $n = 4$ ($M_5C_4T_x$) has been also reported in the solid solutions form.[25] Due to MXenes' top-down synthesis approach, the $M_{n+1}X_n$ composition is derived by the composition of their MAX phase precursors, as shown in Figure 1a–b.

MXenes can be classified into two separate categories based on their transition-metal composition. The first type is mono-transition-metal (mono-M) MXenes (Figure 1), where M layers are made of a single type of a transition metal such as in Ti_2CT_x, V_2CT_x, $Ti_3C_2T_x$, $Nb_4C_3T_x$.[27] Although there are many possible combinations of transition metals and carbon/nitrogen, only 14 mono-M MXenes have been synthesized.[27] A second type of MXenes is known as double transition-metal (DTM) MXenes (**Figure 2**). DTM MXenes are comprised of two distinct transition metals, differentiated by M′ and M″, where their atomic positions are indicated in green and purple, respectively, in Figure 2 and throughout this article. DTM MXenes are further classified by structure into ordered[39,40] (Figure 2a–b) and solid-solution MXenes (Figure 2c).[41,42] In ordered MXenes, the two different transition metals (M′ and M″) occupy the M layers in specific sites, defined as in-plane order (such as $Mo_{4/3}Y_{2/3}CT_x$[40]) or out-of-plane order (such as $Mo_2TiC_2T_x$[39,43] and $Mo_2Ti_2C_3T_x$[39]).

In-plane ordered MXenes, defined by the formula $M'_{4/3}M''_{2/3}XT_x$, are comprised of two different transition metals ordered with alternating sites in each M-layer atomic plane (Figure 2a). Out-of-plane MXenes, defined by the formula $M'_2M''X_2T_x$ or $M'_2M''_2X_3T_x$, are comprised of ordered transition metals in separate atomic planes, where inner layers of M″ transition metals are sandwiched by outer layers of M′ transition metals (Figure 2b). In contrast to ordered MXenes, solid solution MXenes, defined by the formula $(M',M'')_{n+1}C_nT_x$, are comprised of two different transition metals randomly distributed in all M layers, such as $(Ti,V)_2CT_x$, $(Ti,Nb)_3C_2T_x$, and $(Nb,Zr)_4C_3T_x$ (Figure 2c).

To date, all experimentally synthesized and theoretically predicted DTM MXenes are carbides, no DTM MXene nitrides or carbonitrides have been explored. Since the layered structures of DTM MXenes are derived from their parent MAX phases, it is the composition of the MAX phases that governs the composition of DTM MXenes. While more than 20 DTM MXenes have been synthesized from their precursor MAX (Figure 2, highlighted with a solid gradient background), there are many synthesized DTM MAX phases that have not yet been selectively etched to their corresponding DTM MXenes (Figure 2, highlighted with horizontal lines in the background). Similarly, there are additional theoretically predicted DTM MXenes, which have not yet been experimentally realized in MXene or their DTM MAX phase precursor (Figure 2, highlighted with diagonal striped lines in the background).

DTM MXenes add many new compositions to the MXene family, with at least 50 ordered (Figure 2),[39,44,45] and a limitless number of solid-solution MXenes.[41,42,46,47] The possibility of control of the arrangement of transition-metal atoms to form in-plane ordered, out-of-plane ordered, and solid-solution DTM MXenes gives control over the MXenes' electronic, magnetic, electrochemical, optical, and mechanical properties, which is unique to the field of 2D materials. To date, there is no direct transition from the mono-M MXenes to DTM ones, and the synthesis of DTM MXenes is possible only by selective etching of the A-group elements from their DTM MAX phase precursors.

This overview article aims to provide insights into DTM MXenes in terms of their unique structures, formation mechanisms, and subsequent tunable properties. We also provide insights toward future applications and the needed research in this growing field.

In-plane ordered double transition metal MXenes

In-plane ordered DTM MXenes are represented as $M'_{4/3}M''_{2/3}XT_x$ and are one of the latest additions to the MXene family.[40,48] In-plane order is observed only in the thinnest MXene structure, that is, M_2XT_x. Each M layer is occupied by two distinct transition metals M′ and M″, where every two atomic rows of M′ are separated by a row of M″ elements (Figure 2a). M′ (the majority M) is typically V, Nb, Cr, Mo, W, or Mn, and M″ is typically Sc, Y, or Zr. Similar to other MXenes, this unique atomic ordering is derived from their in-plane ordered MAX phase precursors.[49,50] For example, reactive sintering of an elemental mixture of Mo, Y, Al, and C at 1500ºC for 20 h under an argon atmosphere results in an in-plane ordered $Mo_{4/3}Y_{2/3}AlC$ MAX phase (**Figure 3**a).[40] The Al layers are then selectively etched to form in-plane ordered DTM MXenes (Figure 3a–b). The formation of these chemically ordered in-plane structures is primarily attributed to four parameters:[50] (1) A 2:1 stoichiometric ratio of M′:M″ elements, (2) significant difference in atomic radii between M′ and M″, where M″ is larger, (3) the large disparity in electronegativities of the M″ elements and the A layer elements, and (4) an A element with small atomic radius.[51]

In 2019, in-plane ordered DTM MAX phases with rare earth elements as their M″ were synthesized. However, their MXenes have not been made yet.[52]

In the in-plane ordered MAX phase precursors, M″ atoms are slightly extended out of the M layers toward the A layers (Figure 3a),[45] which can lead to two different types of MXenes upon selective etching. A milder etching condition, such as shorter etching time or lower hydrogen fluoride (HF) concentration, results in removal of the A layer only and forms $M'_{4/3}M''_{2/3}CT_x$, illustrated by $Mo_{4/3}Y_{2/3}CT_x$ in Figure 3b. The use of stronger etching conditions, such as longer etching time or higher HF concentration, removes M″ along with the A layers, which forms divacancy ordered MXenes, illustrated by $Mo_{4/3}CT_x$ in Figure 3c.[40] For example, the $Mo_{4/3}Y_{2/3}AlC$ MAX phase was etched in 48 wt.% HF at room temperature for 12 and 72 h to make in-plane ordered DTM $Mo_{4/3}Y_{2/3}CT_x$ and divacancy ordered $Mo_{4/3}CT_x$, respectively.[40] The control of the atomic structure by the presence of ordered rows of M″ versus ordered divacancy adds a unique tool to control the inherent properties, such as electrochemical and electrical conductivity.[40,48]

When used as an electrode in a supercapacitor, the electrochemical performance of Mo containing in-plane ordered MXenes can be tailored through replacement of in-plane ordered DTM MXenes ($Mo_{4/3}Y_{2/3}CT_x$) to in-plane divacancy ordered MXenes ($Mo_{4/3}CT_x$). Figure 3d exhibits the volumetric capacitance of these two MXenes synthesized from two in-plane ordered precursors, $Mo_{4/3}Y_{2/3}AlC$ and $Mo_{4/3}Sc_{2/3}AlC$, respectively. It has been shown that $Mo_{4/3}CT_x$ with ordered divacancy exhibits greater volumetric capacitance in acidic electrolytes compared to $Mo_{4/3}Y_{2/3}CT_x$ (open red squares and open blue circles in Figure 3d). However, in a basic electrolyte, the $Mo_{4/3}Y_{2/3}CT_x$ performed better than $Mo_{4/3}CT_x$ (solid blue circles and solid red squares in Figure 3d), which indicates that electrochemical changes also are electrolyte dependent, as shown through the change in MXenes' capacitance from acidic to basic electrolytes in Figure 3d.[40]

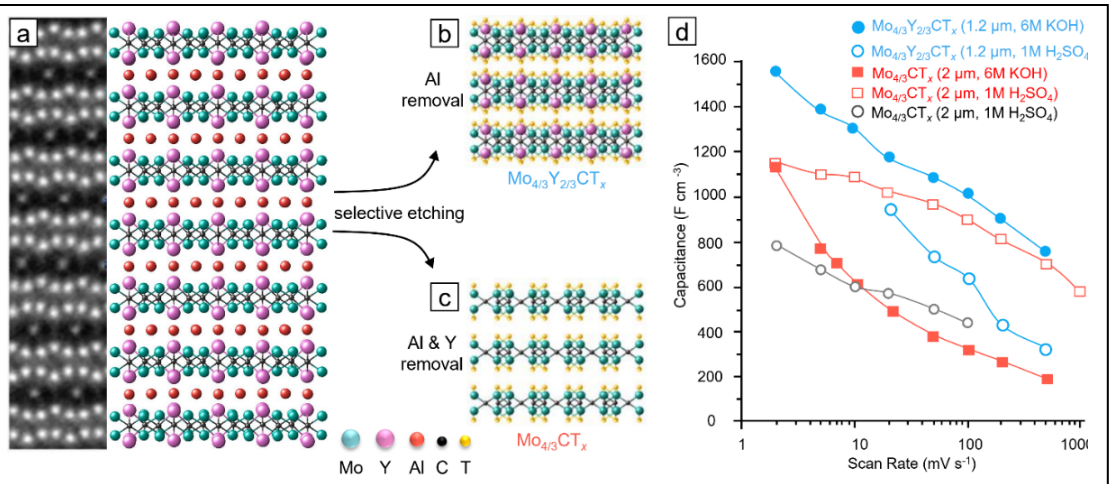

Figure 3. Atomic arrangement of in-plane ordered MXenes and their precursor MAX phase, and their electrochemical performance. (Scale: 1 nm) (a) Scanning transmission electron microscope image[40] (left) and a schematic (right) of $Mo_{4/3}Y_{2/3}AlC$ MAX phase precursor along a [110] zone axis showing its atomic arrangement. (b) Atomic structure of double transition-metal $Mo_{4/3}Y_{2/3}CT_x$ MXene after selective etching of aluminum in 48% HF for 12 h. (c) Atomic structure of divacancy $Mo_{4/3}CT_x$ MXene showing selective etching of both aluminum and in-plane yttrium by longer etching (72 h) in 48% HF. (d) Electrochemical performance of $Mo_{4/3}Y_{2/3}CT_x$ and $Mo_{4/3}CT_x$ in acidic and basic electrolytes showing scan rate and electrolyte dependence of volumetric capacitance. Data for mono-M Mo_2CT_x MXene is shown for comparison.[40]

The changes in the electrochemical behavior of these ordered MXenes are not yet fully understood. These changes could be attributed to the variation of electrochemically active sites or the change of surface terminations concentration and distribution through the introduction of vacancies and the minority M″.[40] $Mo_{4/3}CT_x$ (with divacancies) has shown more–F terminations as compared to Mo_2CT_x.[53] Lower Mo content in $Mo_{4/3}CT_x$ (from 2 to 4/3) leads to shortage of electrons for surface terminations and results in more –F terminations compared to =O terminations.[53] The higher electrical conductivity of $Mo_{4/3}CT_x$ could also contribute to the in-plane divacancy-ordered MXenes' higher electrochemical performace.[48]

Beyond Mo-containing in-plane ordered MXenes, the $W_{4/3}CT_x$ MXene is a promising catalyst for the hydrogen evolution reaction (HER) activity.[54] However, research in electrochemical and catalytic behavior of in-plane ordered DTM and divacancy MXenes is limited. Studies toward further understanding of the fundamentals of charge-transport kinetics in these in-plane ordered DTM MXenes and the effects of vacancies and surface termination compositions on their electrochemical and catalytic performance are necessary, to fully realize their potential for various applications.

Out-of-plane ordered double transition metal MXenes

The second type of ordered DTM MXenes, referred to as out-of-plane ordered, are observed in $M_3C_2T_x$ and $M_4C_3T_x$ (Figure 2b). The out-of-plane order refers to the ordering of transition metals in separate atomic planes, in contrast to the in-plane ordered where transition metals are ordered in an atomic plane. In out-of-plane ordered DTM MXenes, inner layers of M″ transition metals (purple atoms in Figure 2b) are sandwiched by outer layers of M′ transition metals (green atoms in Figure 2b) in a layered structure.[39,55] Like all MXenes, the structural configurations of out-of-plane ordered DTM MXenes begin with synthesis of their precursor MAX phases.[56-58] The only experimentally synthesized out-of-plane ordered DTM MAX phases thus far include Mo_2ScAlC_2,[57] Cr_2VAlC_2,[59] Mo_2TiAlC_2,[56] Cr_2TiAlC_2,[60] Ti_2ZrAlC_2,[61] $Cr_2V_2AlC_3$,[59] and $Mo_2Ti_2AlC_3$.[58] Once ordered MAX phases are selectively etched, their derivative MXenes retain the structural ordering of the corresponding MAX phases.[39,57,62] From out-of-plane ordered MAX phases, the only synthesized DTM out-of-plane MXenes thus far include $Mo_2ScC_2T_x$,[57] $Mo_2TiC_2T_x$,[39] $Cr_2TiC_2T_x$,[39] and $Mo_2Ti_2C_3T_x$.[39]

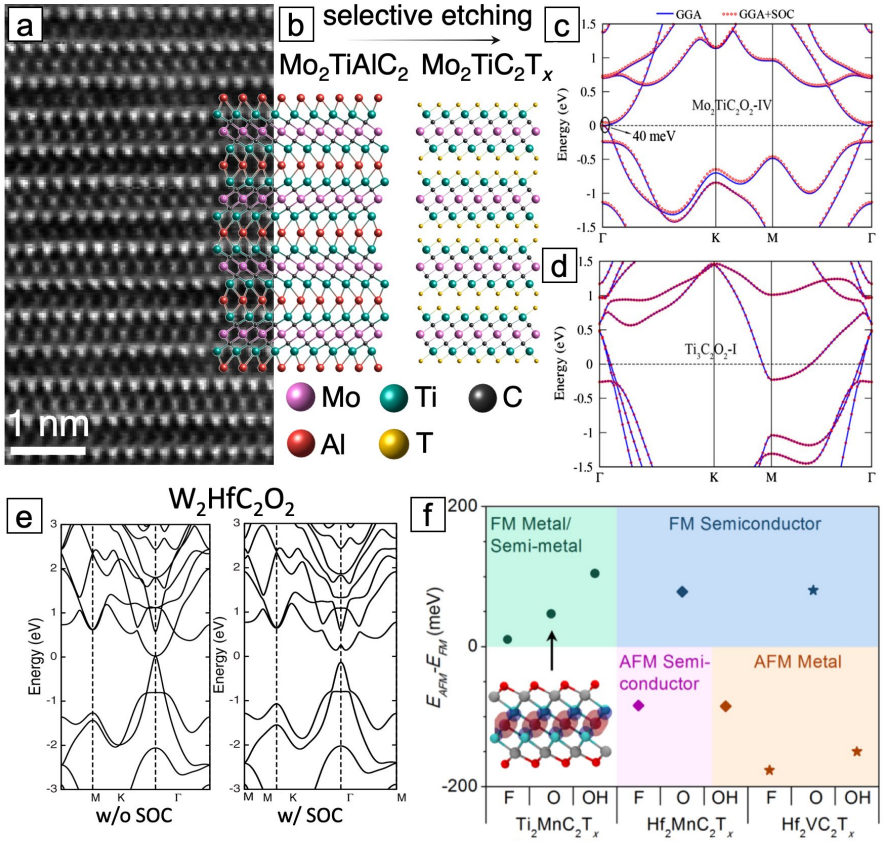

Figure 4. Structure, electronic, and magnetic properties of out-of-plane ordered double transition-metal (DTM) MXenes. (a) High-resolution scanning transmission electron microscope image of Mo_2TiAlC_2 MAX phase.[56] (b) Selective etching process from Mo_2TiAlC_2 to $Mo_2TiC_2T_x$. (c, d) Electronic band structure of (c) $Mo_2TiC_2O_2$ and (d) $Ti_3C_2O_2$, where a slight bandgap in semiconducting $Mo_2TiC_2O_2$ is predicted while metallic behavior is predicted in $Ti_3C_2O_2$.[76] (e) The electronic band structure of $W_2HfC_2O_2$, which highlights the bandgap induced by accounting for spin–orbit coupling (SOC) of electrons in the *d*-orbital of M′ and M″ in the analysis.[55] (f) Ferromagnetism (FM) and antiferromagnetism (AFM) is seen in theoretical out-of-plane DTM MXenes.[64] Both the M′ and M″ transition metals, as well as the surface terminations, significantly affect the magnetic properties of MXenes, where the M′ site determines the interaction with the surface terminations and the M″ site affects the magnitude of magnetic potential.[64]

Figure 4a illustrates a high-resolution scanning transmission electron microscope (STEM) image of Mo_2TiAlC_2 MAX phase,[56] which is then selectively etched in 48 wt.% HF at 55ºC for 48 h to yield the $Mo_2TiC_2T_x$ MXene (Figure 4b). Generally, stable out-of-plane DTM MXenes are predicted to contain Cr, Mo, and W as M′ transition metals and Sc, Ti, Zr, Hf, V, Nb, Ta as M″ transition metals.[63] A complete list of all explored M′ and M″, both experimental and theoretical, is shown in Figure 2b. However, selection of transition-metal pairs beyond current experimentally synthesized out-of-plane ordered DTM MXenes will require researchers to prevent disordered solid solutions of these transition metals in their precursor MAX phases, as we discuss later.[44,63]

The selection of the transition-metal pairs in ordered DTM MAX phase precursors lends considerable control for the electronic, magnetic, optical, and electrochemical properties of their derived ordered out-of-plane DTM MXenes. Significant research has been dedicated to the electronic properties of DTM MXenes, with a combination of theoretical[55,64,65] and experimental results.[15,66,67] In general, the conductivity of mono-M $M_3X_2T_x$ and $M_4X_3T_x$ is metallic, however, some of the out-of-plane ordered DTM MXenes can become semiconductors or semi-metals.[64,68] Figure 4c–d show density function theory (DFT) simulations of the electronic band structures of semiconducting $Mo_2TiC_2O_2$ (40 meV bandgap) and metallic $Ti_3C_2O_2$ with =O surface terminations, respectively.[43] Semiconductor properties in out-of-plane MXenes occur due to spin–orbit coupling (SOC) of electrons in the *d*-orbitals between M′ and M″ transition metals[55] or inducing magnetic ordering of an electron into the M′ transition-metal *d*-orbital.[69] Both effects are further influenced by interactions of M′ and M″ elements with surface terminations,[55,69] where a larger difference in electronegativity between transition metals and surface

terminations increases the potential to form semiconductor MXenes.[70] Figure 4e illustrates the effect of SOC of

electrons in an out-of-plane DTM MXene, where the consideration of this phenomenon changes the prediction of $W_2HfC_2O_2$ from a semi-metal (left panel) to a semiconductor (right panel).[55]

Experimental studies of out-of-plane DTM MXenes have shown that the surface terminations have the largest effect on the properties of exterior M′ transition metals as compared to the inner M″ transition metals.[71] Therefore, the M′ transition-metal and surface terminations in MXenes are important factors to control to form semiconductor MXenes.[43,55,64,72] Theoretical studies predicted M′ transition metals such as Mo, W, Hf, or Cr paired with =O or –F surface terminations to have topological semiconductor bandgaps of 0.119 eV, 0.238 eV, 0.409 eV, and 1.26 eV for $Mo_2TiC_2O_2$, $Hf_2MnC_2O_2$, $W_2HfC_2O_2$, and $Cr_2TiC_2F_x$, respectively.[55,64,69] However, DTM MXenes with uniform surface functional groups (for example, fully F-terminated) have not yet been synthesized, and all synthesized out-of-plane DTM MXenes to date have a mixture of surface terminations and have been electrically conductive.[15,62,66,67,73] Out-of-plane ordered DTM MXenes are less conductive than $Ti_3C_2T_x$, with the highest film conductivity of 1490 $S{\cdot}cm^{-1}$ observed for $Mo_2Ti_2C_3T_x$ (annealed at ~ 500°C) compared to 15,100 $S{\cdot}cm^{-1}$ for $Ti_3C_2T_x$ (annealed at 200°C).[28,66] Additionally, the conductivity of Mo-containing out-of-plane DTM MXene films is shown to be more dependent on interlayer spacing between MXene flakes due to intercalated molecules used in delamination of out-of-plane DTM MXenes as compared to $Ti_3C_2T_x$.[74]

Similar to the electronic properties, the magnetic behavior of ordered MXenes is controlled by both M′ and M″ elements.[64,68,75,76] To date, M′ = Ti, Hf, Cr, and M″ = Mn, V have been explored by first-principles methods for magnetic out-of-plane DTM MXenes. Some of these DTM MXenes have been predicted to be ferromagnetic regardless of surface termination, such as $Ti_2MnC_2T_x$ (Figure 4f).[64] Other out-of-plane ordered DTM MXenes are predicted to be antiferromagnetic, but become ferromagnetic when fully functionalized with =O terminations.[64,65,68,69,75] The combination of surface terminations with M″ in out-of-plane DTM MXenes affects the electron orbitals in M′, where ferromagnetism in MXenes is based on influencing an electron into a *d*-orbital of the M′ transition metal, which changes the oxidation state from M'^{4+} to M'^{3+}.[55,64,69]

Analytical determination of ferromagnetism (FM) versus antiferromagnetism (AFM) can be established by the energy difference $\Delta E = E_{AFM} - E_{FM}$, where positive ΔE represents ferromagnetism and negative ΔE represents antiferromagnetism.[64,68,75] Figure 4f illustrates the effect of the composition of both M′ and M″ transition metals, as well as the surface terminations, on the magnetic properties of MXene.[64] Fluorine surface terminations have lower energy toward ferromagnetism for $Ti_2MnC_2F_2$ and $Hf_2MnC_2F_2$ as compared to –OH and =O terminations.[64] However, the tendency for Ti as M'^{3+} and Hf as M'^{4+} in the presence of Mn and F results in ferromagnetism in $Ti_2MnC_2F_2$ (ΔE = 0.01 eV) and antiferromagnetism in $Hf_2MnC_2F_2$ (ΔE = –

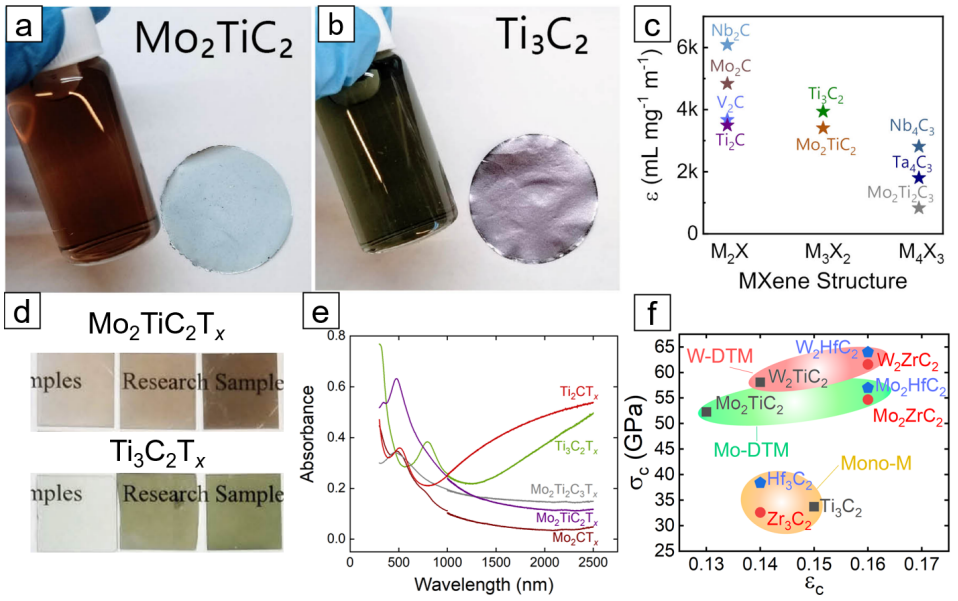

Figure 5. Optical and mechanical properties of out-of-plane ordered double transition-metal (DTM) MXenes. The color of MXene dispersion and its freestanding film of (a) the out-of-plane DTM MXene $Mo_2TiC_2T_x$ and (b) its mono-M counterpart $Ti_3C_2T_x$.[77] (c) The extinction coefficient of colloidal dispersions of M_2X, M_3X_2, and M_4X_3 MXenes, which illustrates the general trend of lower extinction coefficients of out-of-plane DTM MXenes.[77] (d) Increasing thicknesses (left to right) of spray-coated out-of-plane DTM MXene $Mo_2TiC_2T_x$ (above) and its mono-M counterpart $Ti_3C_2T_x$ (below).[77] (e) The absorbance of thin films of Mo and Ti mono-M MXenes combined with their out-of-plane ordered DTM MXenes. (f) The improvement effect of M″ transition metals on effective ideal strength of $M_3C_2T_x$ (assuming monolayer thickness of $M_3C_2O_2$ as 0.83 nm[82]) versus failure strain as compared to mono-M MXenes. MXenes containing Zr, Hf, and Ti as a mono-M or in an M″ site are denoted by red, blue, and gray markers, respectively.[79] The background ovals highlight either the mono-M MXene range in orange, or Mo or W transition metals in M' sites of DTM MXenes as green or red, respectively.

0.084 eV).[64] The change of M″ from Mn to V in $Hf_2M''C_2T_x$ affects the magnitude of magnetism, such as $Hf_2VC_2F_2$ (ΔE = –0.177 eV).[64] No ferromagnetic MXenes have been experimentally reported yet due to the difficulty in synthesizing a precursor MAX phase (such as $Ti_2MnC_2T_x$), or etch the MAX to form MXene (such as $Cr_2V_2C_3T_x$[75]).

Next, we turn our attention to the optical properties of out-of-plane DTM MXenes. In general, MXenes in colloidal solutions and thin films of MXenes have different apparent colors depending on the transition metals used. Furthermore, the effect of the transition metal on the optical properties is more prominent in thinner MXenes M_2XT_x and $M_3X_2T_x$ as compared to thicker $M_4X_3T_x$ MXenes.[77] In out-of-plane DTM MXenes, such as $M'_2M''C_2T_x$, the optical properties are determined mostly by M.′ **Figure 5**a–b show the effect of Ti and Mo as the outer M′ layers in a $M_3C_2T_x$ structure on the color of their respective colloidal dispersions and films, while keeping the M″ as Ti in both MXenes.[77] Figure 5c shows that colloidal out-of-plane DTM MXenes have lower extinction coefficients (at λ = 200 nm) compared to their mono-M MXene counterparts in both $M_3X_2T_x$ and $M_4X_3T_x$ (for example, 3500 $mg^{-1}mL^{-1}$ in $Mo_2TiC_2T_x$ compared to 4000 $mg^{-1}mL^{-1}$ $Ti_3C_2T_x$).[77] Similar to applications of $Ti_3C_2T_x$ as transparent, highly conductive thin films,[78] semiconductor out-of-plane DTM MXenes, if synthesized, could be used as transparent, semiconductor thin films. Figure 5d shows spray-coated films of a DTM $Mo_2TiC_2T_x$, and a mono-M $Ti_3C_2T_x$ and similarly displays the effect of changing transition metal composition on the color of MXene.[77] Figure 5e highlights the absorbance of spray-coated thin films over a range of wavelengths (at λ = 200 nm to 2500 nm).[77]

Currently, there has been no experimental determination of the mechanical properties of DTM MXenes. However, a DFT study predicted higher effective strengths for out-of-plane ordered DTM MXenes as compared to their mono-M counterparts.[79] In this example, when Mo and W are in M′ sites in $M'_2M''C_2O_2$ (M″: Ti, Zr, Hf) the 2D strengths were increased on average by 60% and 77%, respectively, compared to their mono-M $M_3C_2O_2$ MXenes (M: Ti, Zr, Hf).[79] Figure 5f summarizes the predictions of the strength versus critical strain of ordered out-of-plane DTM MXenes. Although no DFT has been performed on higher order out-of-plane DTM MXenes (e.g., $M'_2M''_2X_3$), increasing thickness (M_3X_2 to M_4X_3) tends to reduce the effective mechanical properties.[80-82] Nevertheless, MXenes currently rank as the stiffest solution-processable nanomaterial,[19,20] and the improved mechanical properties of out-of-plane ordered DTM MXenes over their mono-M counterparts illustrates the promise for out-of-plane ordered DTM MXenes in this area.

Random solid solution double transition metal MXenes

In contrast to ordered MXenes, solid-solution MXenes exhibit random distribution of two different transition metals in M-sites (Figure 2c). While ordered DTM structures are unique to MAX phases and MXenes among all known materials, solid solutions DTM MXenes are

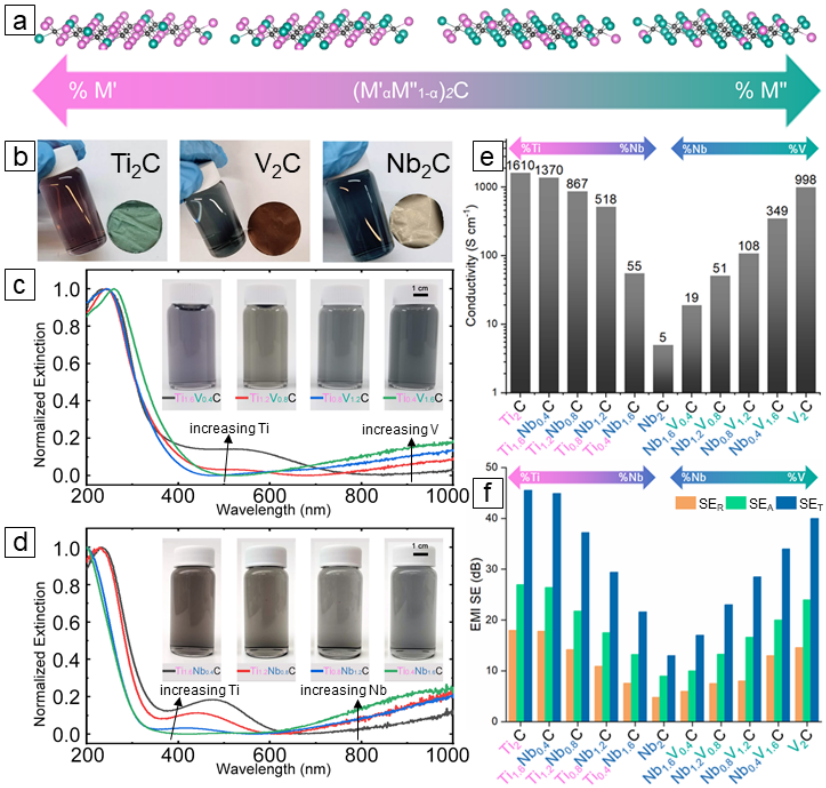

Figure 6. Solid-solution MXenes with tunable properties. (a) Schematic representation of the $(M'_\alpha M''_{1-\alpha})_2CT_x$ solid-solution MXenes system with various M':M" stoichiometric ratios.[77] T_x is not shown in the schematic for simplicity. (b) Dispersed mono-M MXenes Ti_2C (left), V_2C (middle), and Nb_2C (right).[77] (c) Digital image and corresponding normalized optical extinction spectra of the $(Ti_\alpha V_{1-\alpha})_2C$ solid-solution system changing from Ti-rich to V-rich.[77] (d) Digital image and corresponding normalized optical extinction spectra of the $(Ti_\alpha Nb_{1-\alpha})_2C$ solid-solution system changing from Ti-rich to Nb-rich.[77] (e) Electrical conductivities of solid-solution MXenes as a function of varying M':M" stoichiometric ratios. (f) The average electromagnetic interference shielding effectiveness (EMI SE) of different MXene films (5 ± 0.3-μm thick) in the 8.2−12.4 GHz range, showing the reflection (SE_R in orange) and absorption (SE_A in green) contributions, and the total SE (SE_T in blue).[73]

similar to solid solutions in other materials, such as bulk carbides and nitrides[83] or other 2D materials, for example, transition-metal dichalcogenides.[84,85] The control of stoichiometric ratio of M′ to M″ (M′:M′) provides continuous control over the MXenes' structures and properties. Solid-solution MXenes have been reported for all groups of MXenes, M_2CT_x,[47] $M_3C_2T_x$,[42] $M_4C_3T_x$,[41] and even $M_5C_4T_x$.[25] $M_5C_4T_x$ is the highest order of MXenes to date, and has only been observed as solid-solution MXenes.[25] Unlike ordered MXenes, where only a certain stoichiometric ratio of M′:M″ leads to the formation of ordered MAX phase precursors, solid-solution MXenes and their precursor MAX phases encompass a large range of M′:M″. Through control of the stoichiometric ratio of two transition-metal in solid-solution MXenes, $(M'_\alpha M''_{1-\alpha})_{n+1}C_nT_x$ ($0 < \alpha < 1$), their electrochemical,[41,46] catalytic,[42] electrical,[73] and optical[77] properties can be tuned between the properties of their two representative mono-M MXenes. **Figure 6**a shows schematics of solid-solution MXenes as $(M'_\alpha M''_{1-\alpha})_2CT_x$ with different values for α, which changes their M′:M″ ratios. Surface terminations are not shown for simplicity. Figure 6b–d show the control of optical properties by change of the stoichiometric ratio of M′:M″ for two $(M'_\alpha M''_{1-\alpha})_2CT_x$ solid-solution phases, $(Ti_\alpha V_{1-\alpha})_2CT_x$, and $(Ti_\alpha Nb_{1-\alpha})_2CT_x$. The optical properties of the colloidal solid-solution MXenes (Figure 6c–d) varies between their individual mono-M MXenes (Figure 6b). Both $(Ti,V)_2C$ and $(Ti,Nb)_2C$ show a similar trend in their optical properties, through changes in Ti:V or Ti:Nb ratios. In $(Ti,V)_2C$, the extinction peak position at 550 nm observed in Ti-rich samples disappeared with increasing V incorporation (Figure 6c). In $(Ti,Nb)_2C$ the extinction peak at around 500 nm shifts to the left (410 nm in $Ti_{0.8}Nb_{1.2}C$) and disappears by further increasing the Nb content (Figure 6d). In both cases, the addition of V or Nb leads to an increase in near infrared (above 700 nm) extinction.[77]

Similarly, the electronic conductivity and EMI shielding effectiveness of $(Ti_\alpha Nb_{1-\alpha})_2CT_x$ and $(Nb_\alpha V_{1-\alpha})_2CT_x$ solid-solution MXenes can be tuned between Ti_2CT_x and Nb_2CT_x, or Nb_2CT_x and V_2CT_x, based on their M′:M″ atomic ratio (Figure 6e–f). For example, the electrical conductivity can be tuned between 5 to 1610 $S \cdot cm^{-1}$ through variation of α from 0 to 1 in $(Ti_\alpha Nb_{1-\alpha})_2CT_x$.[73] This is similarly seen in thicker MXenes such as in $M_4X_3T_x$ structures. For example, in $(Mo_\alpha V_{1-\alpha})_4C_3T_x$ solid-solution MXenes, electrical conductivity shows more than an order of magnitude increase from 15 $S.cm^{-1}$ for $(MoV_3)C_3T_x$ ($\alpha = 0.25$) to 830 $S.cm^{-1}$ for $(Mo_{2.7}V_{1.3})C_3T_x$ ($\alpha = 0.675$).[46] This control of properties by changing the M′:M″ ratio shows the potential of solid-solution MXenes in application-driven design.

Similar to ordered MXenes, the control of stoichiometry in solid-solution MXenes comes from their MAX phase precursors. Although solid-solution MXenes were reported as early as 2012,[12] with more than thousands of predicted compositions of solid solutions,[86] there are a limited number of both experimental and theoretical studies on solid-solution MXenes (Figure 2c). Additionally, many solid-solution MAX phases, such as $(Cr_\alpha Mn_{1-\alpha})_2AlC$, have not yet been etched to MXene.[87] All experimentally reported solid-solution DTM MAX phases where their MXenes are not made yet are marked with horizontal striped background in Figure 2c.

Parameters controlling ordered and solid solution MXene formations

The formation criteria of both ordered MXenes and solid-solution MXenes are necessary to understand the preferred structure of DTM MXenes as ordered or solid solutions of transition metals. The M ordering of MXenes is dependent on total energy or formation energy, which is changed by the choice of transition-metal pairs.[39,44] **Figure 7**a shows the total energy diagram of a selection of $M'_2M''_2C_3$ DTM MXenes with different configurations varied from fully ordered (left) to solid solutions (right).[39] For these specific transition-metal pairs, fully ordered DTM MXene (100% M″ in the outer layers) illustrates lower theoretical total energies as compared to disordered solid solution configurations, which indicates that these ordered configurations are more stable at 0 K.[39]

However, the degree of favorability for ordered versus solid-solution DTM MXene structures depends on the transition-metals pairs. For example, in $Mo_2Ti_2C_3T_x$ MXene, the change of Mo/Ti occupancy in the four M layers from ordered to solid solution increases the total energy by ~0.5 eV (Figure 7a). Due to this large difference in total energy between ordered and disordered Mo-Ti DTM MXenes, $Mo_2Ti_2C_3T_x$ has been synthesized and characterized only as an ordered DTM MXene.[39] In contrast, for a Mo-V-containing DTM MXene $M_4C_3T_x$, the change of total energy from ordered to solid solution is among the smallest (~0.2 eV), as shown Figure 7a. Due to the high heats required to form MAX phases (>1700 K), we speculate that the small difference in total energy between ordered and solid solutions is overcome by the increased effect of entropy by the high thermal energy needed for MAX formation,[44] which results in preference for the transition metal pair Mo-V to form solid solutions. The effect of high heats for formation of precursor MAX phases has been demonstrated experimentally, as all formed Mo-V DTM MXenes to date have been found in solid-solution $(Mo_\alpha V_{1-\alpha})_4C_3T_x$ configurations.[46]

X-ray diffraction (XRD) is one of the tools that can be used to determine which atomic arrangement (ordered versus solid solution) forms in the DTM MAX phase precursors. When a solid solution is formed, changing the M′:M″ stoichiometric ratio results in similar XRD patterns with slightly shifted peaks, due to slight changes in the lattice parameters. For example, by changing the Mo:V ratio in the $(Mo_\alpha V_{1-\alpha})_4AlC_3$ solid solution, peak shifting was observed due to the solid-solution effect (Figure 7b–c).[46] By increasing the V element content, the (002) peak of $(Mo_\alpha V_{1-\alpha})_4AlC_3$ shifted to higher angles (Figure 7c).

In contrast, when ordered DTM MAX phases are formed, changing the M′:M″ ratios gives different XRD

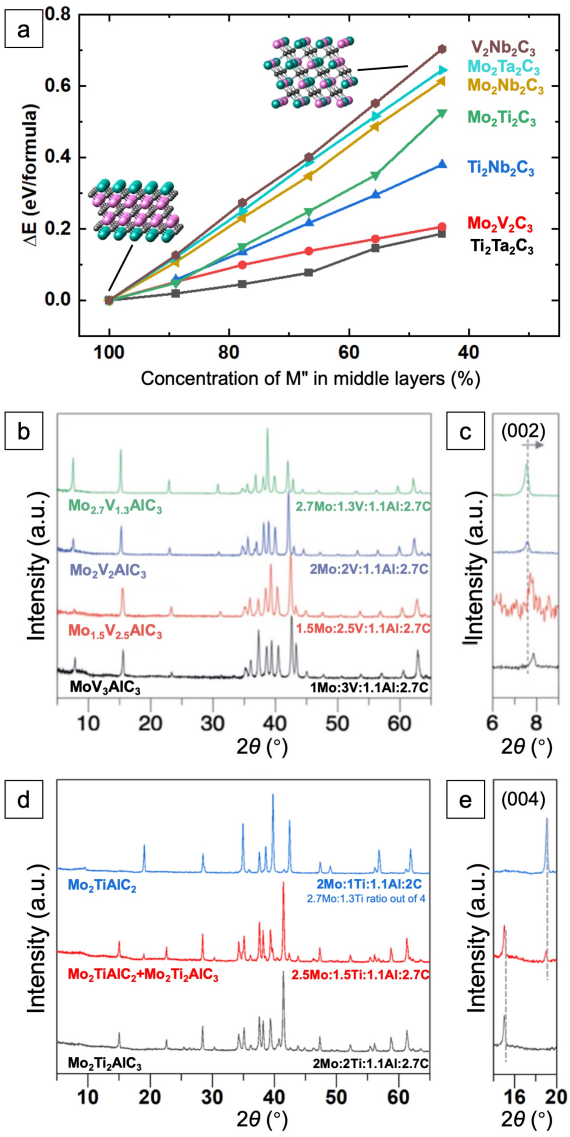

Figure 7. Predicted stability of double transition-metal (DTM) MXenes and x-ray diffraction (XRD) patterns of DTM MAX phases. (a) Total energy diagrams of calculated $M'_2M''_2C_3$ MXenes with respect to concentration of M" in the middle layers.[39] Predictions of MXene stabilities were conducted at 0 K. (b) XRD patterns of $(Mo_\alpha V_{1-\alpha})_4AlC_3$ MAX phases.[46] (c) Close view of (002) peaks shifting to the right with increasing V content. (d) XRD patterns of ordered Mo_2TiAlC_2 and $Mo_2Ti_2AlC_3$ MAX phases.[58] (e) Close view of (004) peaks, showing that not following the stoichiometric ratio leads to formation of Mo_2TiAlC_2 and $Mo_2Ti_2AlC_3$ MAX phases mixture (middle pattern).

spectra indicating different phase formation. For example, the XRD patterns of three phases with Mo:Ti ratios of 2.7:1.3, 2.5:1.5, and 2:2 are shown in Figure 7d. All three were sintered under similar conditions. However, each leads to either ordered M_3AlC_2 for Mo:Ti 2.7:1.3 (top pattern in Figure 7d) or ordered M_4AlC_3 for Mo:Ti 2:2 ratio (bottom pattern in Figure 7d). The (004) peaks in their XRD patterns (Figure 7e) clearly show that not following the stoichiometric ratio (for example, Mo:Ti = 2.5:1.5) leads to a mixture containing two ordered MAX phases without any peak shifting.[58]

According to recent theoretical study of DTM MAX, out-of-plane ordered structures are predicted to form out of combinations of M′ and M″, which have a large difference in electronegativity (>0.4), an increased difference in atomic radii (0.2 Å), as well as an increased difference in electronegativity between M′ and the A-group element in the MAX phase precursor.[63] Combinations of transition-metal pairs, which do not follow these general trends for ordered DTM MAX formation, tend to form solid-solution structures.[63] Based on these general trends, solid-solution structures are more likely in phases comprised of transition-metal pairs from groups 3–5 of the periodic table (Sc, Ti, V, Zr, Nb, Hf, and Ta).[63]

Future scope and outlook

Double transition-metal MXenes are in their early stages of research and development since there are many compositions yet to be explored experimentally or computationally. Although more than 50 ordered DTM compositions are theoretically stable in both MAX phases and MXenes, only 10 have been experimentally realized (Figure 2a-b). Even in computational research, the properties and structures of few ordered DTM MXenes have been investigated. With the addition of solid-solution DTM MXenes, the number of composition possibilities and potential for tunable properties becomes limitless, which opens new approaches to the design of 2D materials with fine-tuned properties for specific applications. Exploration of the effects of transition metals on properties of MXenes by theoretical methods can give guidance for future studies on theory-guided-synthesis of new MXenes.

The number of possibilities for DTM MXenes increases in light of recent scientific advances made in MAX phase precursors. Currently, there are ordered and solid-solution DTM MAX phases which have been synthesized, but not yet etched to their respective DTM MXenes (marked with horizontal striped background in Figure 2). Additionally, current research has only been carried out on DTM MXenes made from carbide MAX phases, and no nitride or carbonitride DTM MXenes have been explored, although some mono-M nitride[88] and carbonitride[89] MXenes have been experimentally realized. As nitride and carbonitride MXenes have shown different properties than their carbide counterparts in energy-storage applications,[90-92] it is expected that nitrogen or carbon/nitrogen as X in MXene will affect the properties of potential DTM nitride/carbonitride MXenes. Future computational studies should investigate the use of nitrogen or carbon/nitrogen as X in DTM MXenes, and their effects on MXenes structures and properties.

The possibilities for DTM MXenes can be further expanded with the addition of tunable surface terminations. Full control over MXenes' termination compositions is yet to be experimentally realized despite DFT studies

suggesting unique properties, such as magnetic[64] or topological insulation.[55] The first superconductive mono-M Nb_2CCl_2 MXene was synthesized recently by creating a uniform –Cl surface terminations, which shows the promise of controlling MXenes' surface terminations.[38] With the consideration of surface terminations, the control of the ratio of transition metal pairs in solid solutions, and the addition of DTM MXene nitrides or carbonitrides, the number of possible DTM MXene compositions becomes limitless.

Additionally, all DTM MXenes have been made from aluminum-containing MAX phases to date.[45] Recently, new methods of selective etching show that MXenes from non-Al-based MAX phases can be successfully synthesized.[36,93] The use of A-group elements with different electronegativities could allow formation of in-plane, out-of-plane, or solid-solution DTM MAX phases comprised of transition-metal pairs which do not form these structures when Al is used as the A-group element. Additionally, etching of other A-group elements allows the synthesis of Mn-containing MXenes from already available Mn-containing MAX phases.[87,94] In 2019, the family of in-plane ordered DTM MAX phases expanded to include rare-earth elements, such as Ce, Pr, Nd, Sm, Gd, Tb, Dy, Ho, Er, Tm, and Lu.[52] If rare-earth MXenes can be realized through controlled etching conditions, it opens the door to *f*-block element MXenes. This could lead to novel behavior, which has not yet been identified in MXenes. Finally, MXenes which contain three or more transition metals (multi-principal element MXenes) have not yet been explored computationally or experimentally yet, which can expand MXenes toward high-entropy 2D materials. The addition of more complexity in MXene compositions could give new means of controlling properties.

Summary

The family of MXenes has now expanded to include in-plane ordered, out-of-plane ordered, and disordered DTM MXenes. This overview article has summarized the general rules of formation of each DTM MXene structure and their tunable properties based on transition-metal composition. All three types of DTM MXenes have illustrated behavior not yet seen in mono-M MXenes, which indicates promise for the use of DTM MXenes in a variety of novel applications. The control of the composition of DTM MXenes' precursor MAX phase allows researchers to tune the performance of MXenes for a range of applications, from supercapacitors, semiconductors, transparent electronics, nano-magnets, and structural materials. The addition of DTM MXenes to the category of 2D materials has expanded the design scope of nanomaterials to meet the demands of an evolving technological sphere.

Acknowledgement

B.A. acknowledges startup funding from the Department of Mechanical and Energy Engineering and Purdue School of Engineering and Technology of IUPUI.

References

1. K. S. Novoselov, A. K. Geim, S. V. Morozov, D. Jiang, Y. Zhang, S. V. Dubonos, I. V. Grigorieva & A. A. Firsov. Electric field effect in atomically thin carbon films. *Science.* **306**, 666-669 (2004).
2. X. Zhang, L. Hou, A. Ciesielski & P. Samorì. 2D materials beyond graphene for high-performance energy storage applications. *Adv. Energy Mater.* **6**, 1600671 (2016).
3. E. Pomerantseva & Y. Gogotsi. Two-dimensional heterostructures for energy storage. *Nat. Energy.* **2**, 1-6 (2017).
4. B. Xu, S. Qi, M. Jin, X. Cai, L. Lai, Z. Sun, X. Han, Z. Lin, H. Shao & P. Peng. 2020 roadmap on two-dimensional materials for energy storage and conversion. *Chinese Chemical Letters* **30**, 2053-2064 (2019).
5. H. Kim & H. N. Alshareef. MXetronics: MXene-Enabled Electronic and Photonic Devices. *ACS Mater. Lett.* **2**, 55-70 (2019).
6. L. Ding, Y. Wei, Y. Wang, H. Chen, J. Caro & H. Wang. A two-dimensional lamellar membrane: MXene nanosheet stacks. *Angew. Chem. Int. Ed.* **56**, 1825-1829 (2017).
7. P. Sun, M. Zhu, K. Wang, M. Zhong, J. Wei, D. Wu, Z. Xu & H. Zhu. Selective ion penetration of graphene oxide membranes. *ACS Nano.* **7**, 428-437 (2013).
8. T. Y. Ma, J. L. Cao, M. Jaroniec & S. Z. Qiao. Interacting carbon nitride and titanium carbide nanosheets for high-performance oxygen evolution. *Angew. Chem. Int. Ed.* **55**, 1138-1142 (2016).
9. W. Yuan & G. Shi. Graphene-based gas sensors. *J. Mater. Chem. A.* **1**, 10078-10091 (2013).
10. W. Yang, K. R. Ratinac, S. P. Ringer, P. Thordarson, J. J. Gooding & F. Braet. Carbon nanomaterials in biosensors: should you use nanotubes or graphene? *Angew. Chem. Int. Ed.* **49**, 2114-2138 (2010).
11. M. Naguib, M. Kurtoglu, V. Presser, J. Lu, J. Niu, M. Heon, L. Hultman, Y. Gogotsi & M. W. Barsoum. Two-Dimensional Nanocrystals Produced by Exfoliation of Ti_3AlC_2. *Adv. Mater.* **23**, 4248-4253, doi:10.1002/adma.201102306 (2011).
12. M. Naguib, O. Mashtalir, J. Carle, V. Presser, J. Lu, L. Hultman, Y. Gogotsi & M. W. Barsoum. Two-Dimensional Transition Metal Carbides. *ACS Nano* **6**, 1322-1331, doi:10.1021/nn204153h (2012).
13. M. Khazaei, M. Arai, T. Sasaki, C.-Y. Chung, N. S. Venkataramanan, M. Estili, Y. Sakka & Y. Kawazoe. Novel Electronic and Magnetic Properties of Two-Dimensional Transition Metal Carbides and Nitrides. *Adv. Funct. Mater.* **23**, 2185-2192, doi:10.1002/adfm.201202502 (2013).
14. M. Khazaei, A. Ranjbar, M. Arai, T. Sasaki & S. Yunoki. Electronic properties and applications of MXenes: a theoretical review. *Journal of Materials Chemistry C* **5**, 2488-2503 (2017).
15. B. Anasori, C. Shi, E. J. Moon, Y. Xie, C. A. Voigt, P. R. Kent, S. J. May, S. J. Billinge, M. W. Barsoum & Y. Gogotsi. Control of electronic properties of 2D carbides (MXenes) by manipulating their transition metal layers. *Nanoscale Horiz.* **1**, 227-234 (2016).
16. K. Hantanasirisakul, M. Q. Zhao, P. Urbankowski, J. Halim, B. Anasori, S. Kota, C. E. Ren, M. W. Barsoum & Y. Gogotsi. Fabrication of $Ti_3C_2T_x$ MXene transparent thin films with tunable optoelectronic properties. *Adv. Electron. Mater.* **2**, 1600050 (2016).
17. H. Zhang, G. Yang, X. Zuo, H. Tang, Q. Yang & G. Li. Computational studies on the structural, electronic and optical properties of graphene-like MXenes (M_2CT_2, M= Ti, Zr, Hf; T= O, F, OH) and their potential applications as visible-light driven photocatalysts. *J. Mater. Chem. A.* **4**, 12913-12920 (2016).
18. A. D. Dillon, M. J. Ghidiu, A. L. Krick, J. Griggs, S. J. May, Y. Gogotsi, M. W. Barsoum & A. T. Fafarman. Highly conductive optical quality solution-processed films of 2D titanium carbide. *Adv. Funct. Mater.* **26**, 4162-4168 (2016).
19. A. Lipatov, H. Lu, M. Alhabeb, B. Anasori, A. Gruverman, Y. Gogotsi & A. Sinitskii. Elastic properties of 2D $Ti_3C_2T_x$ MXene monolayers and bilayers. *Sci. Adv.* **4**, eaat0491 (2018).
20. A. Lipatov, M. Alhabeb, H. Lu, S. Zhao, M. J. Loes, N. S. Vorobeva, Y. Dall'Agnese, Y. Gao, A. Gruverman & Y. Gogotsi. Electrical and Elastic Properties of Individual Single-Layer $Nb_4C_3T_x$ MXene Flakes. *Adv. Electron. Mater.* **6**, 1901382 (2020).
21. X.-H. Zha, K. Luo, Q. Li, Q. Huang, J. He, X. Wen & S. Du. Role of the surface effect on the structural, electronic and mechanical properties of the carbide MXenes. *EPL (Europhysics Letters)* **111**, 26007 (2015).
22. M. Alhabeb, K. Maleski, B. Anasori, P. Lelyukh, L. Clark, S. Sin & Y. Gogotsi. Guidelines for Synthesis and Processing of Two-Dimensional

Titanium Carbide ($Ti_3C_2T_x$ MXene). *Chem. Mater.* **29**, 7633-7644, doi:10.1021/acs.chemmater.7b02847 (2017).
23. K. Maleski, V. N. Mochalin & Y. Gogotsi. Dispersions of Two-Dimensional Titanium Carbide MXene in Organic Solvents. *Chem. Mater.* **29**, 1632-1640 (2017).
24. B. Anasori, M. R. Lukatskaya & Y. Gogotsi. 2D metal carbides and nitrides (MXenes) for energy storage. *Nat. Rev. Mater.* **2**, 16098, doi:10.1038/natrevmats.2016.98 (2017).
25. G. Deysher, C. E. Shuck, K. Hantanasirisakul, N. C. Frey, A. C. Foucher, K. Maleski, A. Sarycheva, V. B. Shenoy, E. A. Stach & B. Anasori. Synthesis of Mo_4VAlC_4 MAX Phase and Two-Dimensional Mo_4VC_4 MXene with Five Atomic Layers of Transition Metals. *ACS Nano.* **14**, 204–217 (2020).
26. M. Naguib, V. N. Mochalin, M. W. Barsoum & Y. Gogotsi. 25th anniversary article: MXenes: a new family of two-dimensional materials. *Adv. Mater.* **26**, 992-1005 (2014).
27. Y. Gogotsi & B. Anasori. The Rise of MXenes. *ACS Nano* **13**, 8491-8494, doi:10.1021/acsnano.9b06394 (2019).
28. J. Zhang, N. Kong, S. Uzun, A. Levitt, S. Seyedin, P. A. Lynch, S. Qin, M. Han, W. Yang & J. Liu. Scalable Manufacturing of Free-Standing, Strong $Ti_3C_2T_x$ MXene Films with Outstanding Conductivity. *Adv. Mater.* **32**, 2001093 (2020).
29. F. Shahzad, M. Alhabeb, C. B. Hatter, B. Anasori, S. M. Hong, C. M. Koo & Y. Gogotsi. Electromagnetic interference shielding with 2D transition metal carbides (MXenes). *Science.* **353**, 1137-1140, doi:10.1126/science.aag2421 (2016).
30. M. Radovic & M. W. Barsoum. MAX phases: Bridging the gap between metals and ceramics. *AMERICAN CERAMIC SOCIETY BULLETIN* **92**, 20-27 (2013).
31. J. Zhou, X. Zha, F. Y. Chen, Q. Ye, P. Eklund, S. Du & Q. Huang. A two-dimensional zirconium carbide by selective etching of Al_3C_3 from nanolaminated $Zr_3Al_3C_5$. *Angew. Chem. Int. Ed.* **55**, 5008-5013 (2016).
32. M. Sokol, V. Natu, S. Kota & M. W. Barsoum. On the Chemical Diversity of the MAX Phases. *Trends Chem.* **1**, 210-223, doi:10.1016/j.trechm.2019.02.016 (2019).
33. M. Khazaei, A. Ranjbar, K. Esfarjani, D. Bogdanovski, R. Dronskowski & S. Yunoki. Insights into exfoliation possibility of MAX phases to MXenes. *Physical Chemistry Chemical Physics* **20**, 8579-8592 (2018).
34. M. A. Hope, A. C. Forse, K. J. Griffith, M. R. Lukatskaya, M. Ghidiu, Y. Gogotsi & C. P. Grey. NMR Reveals the Surface Functionalisation of Ti_3C_2 MXene. *Phys. Chem. Chem. Phys.* **18**, 5099 (2016).
35. X. Wang, X. Shen, Y. Gao, Z. Wang, R. Yu & L. Chen. Atomic-scale recognition of surface structure and intercalation mechanism of Ti_3C_2X. *J. Am. Chem. Soc.* **137**, 2715-2721 (2015).
36. Y. Li, H. Shao, Z. Lin, J. Lu, L. Liu, B. Duployer, P. O. Persson, P. Eklund, L. Hultman & M. Li. A general Lewis acidic etching route for preparing MXenes with enhanced electrochemical performance in non-aqueous electrolyte. *Nat. Mater.*, 1-6 (2020).
37. I. Persson, L.-Å. Näslund, J. Halim, M. W. Barsoum, V. Darakchieva, J. Palisaitis, J. Rosen & P. O. Å. Persson. On the organization and thermal behavior of functional groups on Ti3C2 MXene surfaces in vacuum. *2D Materials* **5**, 015002 (2017).
38. V. Kamysbayev, A. S. Filatov, H. Hu, X. Rui, F. Lagunas, D. Wang, R. F. Klie & D. V. Talapin. Covalent surface modifications and superconductivity of two-dimensional metal carbide MXenes. *Science*, eaba8311 (2020).
39. B. Anasori, Y. Xie, M. Beidaghi, J. Lu, B. C. Hosler, L. Hultman, P. R. C. Kent, Y. Gogotsi & M. W. Barsoum. Two-Dimensional, Ordered, Double Transition Metals Carbides (MXenes). *ACS Nano* **9**, 9507-9516, doi:10.1021/acsnano.5b03591 (2015).
40. I. Persson, A. el Ghazaly, Q. Tao, J. Halim, S. Kota, V. Darakchieva, J. Palisaitis, M. W. Barsoum, J. Rosen & P. O. A. Persson. Tailoring Structure, Composition, and Energy Storage Properties of MXenes from Selective Etching of In-Plane, Chemically Ordered MAX Phases. *Small* **14**, 1703676, doi:10.1002/smll.201703676 (2018).
41. J. Yang, M. Naguib, M. Ghidiu, L. M. Pan, J. Gu, J. Nanda, J. Halim, Y. Gogotsi & M. W. Barsoum. Two-Dimensional Nb-Based M_4C_3 Solid Solutions (MXenes). *J. Am. Ceram. Soc.* **99**, 660-666 (2016).
42. Z. Shen, Z. Wang, M. Zhang, M. Gao, J. Hu, F. Du, Y. Liu & H. Pan. A novel solid-solution MXene $(Ti_{0.5}V_{0.5})_3C_2$ with high catalytic activity for hydrogen storage in MgH_2. *Materialia.* **1**, 114-120 (2018).
43. L. Li. Lattice dynamics and electronic structures of $Ti_3C_2O_2$ and $Mo_2TiC_2O_2$ (MXenes): The effect of Mo substitution. *Comput. Mater. Sci.* **124**, 8-14 (2016).
44. T. L. Tan, H. M. Jin, M. B. Sullivan, B. Anasori & Y. Gogotsi. High-Throughput Survey of Ordering Configurations in MXene Alloys Across Compositions and Temperatures. *ACS Nano.* **11**, 4407-4418, doi:10.1021/acsnano.6b08227 (2017).
45. J. Rosen, M. Dahlqvist, Q. Tao & L. Hultman. in *2D Metal Carbides and Nitrides (MXenes)* (eds Babak Anasori & Yury Gogotsi) 37-52 (Springer, 2019).
46. D. Pinto, B. Anasori, H. Avireddy, C. E. Shuck, K. Hantanasirisakul, G. Deysher, J. R. Morante, W. Porzio, H. N. Alshareef & Y. Gogotsi. Synthesis and Electrochemical Properties of 2D Molybdenum Vanadium Carbides–Solid Solution MXenes. *J. Mater. Chem. A.* **8**, 8957-8968 (2020).
47. S. Yazdanparast, S. Soltanmohammad, A. Fash-White, G. Tucker & G. L. Brennecka. Synthesis and Surface Chemistry of 2D TiVC Solid-Solution MXenes. *ACS Appl. Mater. Interfaces.* **12**, 20129–20137 (2020).
48. Q. Tao, M. Dahlqvist, J. Lu, S. Kota, R. Meshkian, J. Halim, J. Palisaitis, L. Hultman, M. W. Barsoum & P. O. Persson. Two-dimensional $Mo_{1.33}C$ MXene with divacancy ordering prepared from parent 3D laminate with in-plane chemical ordering. *Nat. Commun.* **8**, 14949 (2017).
49. L. Chen, M. Dahlqvist, T. Lapauw, B. Tunca, F. Wang, J. Lu, R. Meshkian, K. Lambrinou, B. Blanpain & J. Vleugels. Theoretical prediction and synthesis of $(Cr_{2/3}Zr_{1/3})_2AlC$ i-MAX phase. *Inorg. Chem.* **57**, 6237-6244 (2018).
50. M. Dahlqvist, J. Lu, R. Meshkian, Q. Tao, L. Hultman & J. Rosen. Prediction and synthesis of a family of atomic laminate phases with Kagomé-like and in-plane chemical ordering. *Sci. Adv.* **3**, e1700642 (2017).
51. M. Dahlqvist, A. Petruhins, J. Lu, L. Hultman & J. Rosen. Origin of Chemically Ordered Atomic Laminates (i-MAX): Expanding the Elemental Space by a Theoretical/Experimental Approach. *ACS Nano.* **12**, 7761-7770, doi:10.1021/acsnano.8b01774 (2018).
52. Q. Tao, J. Lu, M. Dahlqvist, A. Mockute, S. Calder, A. Petruhins, R. Meshkian, O. Rivin, D. Potashnikov, E. a. N. Caspi, H. Shaked, A. Hoser, C. Opagiste, R.-M. Galera, R. Salikhov, U. Wiedwald, C. Ritter, A. R. Wildes, B. Johansson, L. Hultman, M. Farle, M. W. Barsoum & J. Rosen. Atomically Layered and Ordered Rare-Earth i-MAX Phases: A New Class of Magnetic Quaternary Compounds. *Chem. Mater.* **31**, 2476-2485, doi:10.1021/acs.chemmater.8b05298 (2019).
53. H. Lind, J. Halim, S. Simak & J. Rosén. Investigation of vacancy-ordered $Mo_{1.33}C$ MXene from first principles and x-ray photoelectron spectroscopy. *Physical Review Materials* **1**, 044002 (2017).
54. R. Meshkian, M. Dahlqvist, J. Lu, B. Wickman, J. Halim, J. Thornberg, Q. Tao, S. Li, S. Intikhab, J. Snyder, M. W. Barsoum, M. Yildizhan, J. Palisaitis, L. Hultman, P. O. A. Persson & J. Rosen. W-Based Atomic Laminates and Their 2D Derivative $W_{1.33}C$ MXene with Vacancy Ordering. *Adv. Mater.* **30**, 1706409, doi:10.1002/adma.201706409 (2018).
55. M. Khazaei, A. Ranjbar, M. Arai & S. Yunoki. Topological insulators in the ordered double transition metals $M'_2M''C_2$ MXenes (M'=Mo, W; M''=Ti, Zr, Hf). *Phys. Rev. B.* **94**, 125152, doi:10.1103/physrevb.94.125152 (2016).
56. B. Anasori, J. Halim, J. Lu, C. A. Voigt, L. Hultman & M. W. Barsoum. Mo_2TiAlC_2: A new ordered layered ternary carbide. *Scr. Mater.* **101**, 5-7 (2015).
57. R. Meshkian, Q. Tao, M. Dahlqvist, J. Lu, L. Hultman & J. Rosen. Theoretical stability and materials synthesis of a chemically ordered MAX phase, Mo_2ScAlC_2, and its two-dimensional derivate Mo_2ScC_2 MXene. *Acta Mater.* **125**, 476-480 (2017).
58. B. Anasori, M. Dahlqvist, J. Halim, E. J. Moon, J. Lu, B. C. Hosler, E. a. N. Caspi, S. J. May, L. Hultman & P. Eklund. Experimental and theoretical characterization of ordered MAX phases Mo_2TiAlC_2 and $Mo_2Ti_2AlC_3$. *J. Appl. Phys.* **118**, 094304 (2015).
59. E. N. Caspi, P. Chartier, F. Porcher, F. Damay & T. Cabioc'h. Ordering of (Cr,V) Layers in Nanolamellar $(Cr_{0.5}V_{0.5})_{n+1}AlC_n$ Compounds. *Mater. Res. Lett.*, 1-7, doi:http://dx.doi.org/10.1080/21663831.2014.975294 (2014).

60. Z. Liu, L. Zheng, L. Sun, Y. Qian, J. Wang & M. Li. $(Cr_{2/3}Ti_{1/3})_3AlC_2$ and $(Cr_{5/8}Ti_{3/8})_4AlC_3$: New MAX-phase Compounds in Ti-Cr-Al-C System. *J. Am. Ceram. Soc.* **97**, 67-69 (2014).
61. B. Tunca, T. Lapauw, O. M. Karakulina, M. Batuk, T. Cabioc'h, J. Hadermann, R. Delville, K. Lambrinou & J. Vleugels. Synthesis of MAX phases in the Zr-Ti-Al-C system. *Inorg. Chem.* **56**, 3489-3498 (2017).
62. G. Lui, V. Natu, T. Shi, M. W. Barsoum & L. V. Titova. Two-Dimensional MXenes $Mo_2Ti_2C_3T_z$ and $Mo_2TiC_2T_z$: Microscopic Conductivity and Dynamics of Photoexcited Carriers. *ACS Appl. Energy Mater.* **3**, 1530-1539, doi:10.1021/acsaem.9b01966 (2020).
63. M. Dahlqvist & J. Rosen. Predictive theoretical screening of phase stability for chemical order and disorder in quaternary 312 and 413 MAX phases. *Nanoscale* **12**, 785-794 (2020).
64. L. Dong, H. Kumar, B. Anasori, Y. Gogotsi & V. B. Shenoy. Rational Design of Two-Dimensional Metallic and Semiconducting Spintronic Materials Based on Ordered Double-Transition-Metal MXenes. *J. Phys. Chem. Lett.* **8**, 422-428, doi:10.1021/acs.jpclett.6b02751 (2017).
65. W. W. Sun, Y. Xie & P. R. C. Kent. Double transition metal MXenes with wide band gaps and novel magnetic properties. *Nanoscale* **10**, 11962-11968, doi:10.1039/c8nr00513c (2018).
66. H. Kim, B. Anasori, Y. Gogotsi & H. N. Alshareef. Thermoelectric Properties of Two-Dimensional Molybdenum-Based MXenes. *Chem. Mater.* **29**, 6472-6479, doi:10.1021/acs.chemmater.7b02056 (2017).
67. J. L. Hart, K. Hantanasirisakul, A. C. Lang, B. Anasori, D. Pinto, Y. Pivak, J. T. van Omme, S. J. May, Y. Gogotsi & M. L. Taheri. Control of MXenes' electronic properties through termination and intercalation. *Nat. Commun.* **10**, 1-10 (2019).
68. E. M. D. Siriwardane & D. Cakir. Strain engineering of electronic and magnetic properties of double-transition metal ferromagnetic semiconductor MXenes. *J. Appl. Phys.* **125**, 082527, doi:10.1063/1.5054131 (2019).
69. J. J. He, G. Q. Ding, C. Y. Zhong, S. Li, D. F. Li & G. Zhang. Cr_2TiC_2-based double MXenes: novel 2D bipolar antiferromagnetic semiconductor with gate-controllable spin orientation toward antiferromagnetic spintronics. *Nanoscale* **11**, 356-364, doi:10.1039/c8nr07692h (2019).
70. A. C. Rajan, A. Mishra, S. Satsangi, R. Vaish, H. Mizuseki, K.-R. Lee & A. K. Singh. Machine-learning-assisted accurate band gap predictions of functionalized MXene. *Chem. Mater.* **30**, 4031-4038 (2018).
71. Y. Yang, K. Hantanasirisakul, N. Frey, B. Anasori, R. Green, P. Rogge, I. Waluyo, A. Hunt, P. Shafer, E. Arenholz, V. Shenoy, Y. Gogotsi & S. May. Distinguishing electronic contributions of surface and sub-surface transition metal atoms in Ti-based MXenes. *2D Mater.* **7**, 025015 (2020).
72. Z. H. Fu, Z. R. Liu, D. Legut, T. C. Germann, C. Si, S. Y. Du, J. S. Francisco & R. F. Zhang. Designing Flexible Quantum Spin Hall Insulators through 2D Ordered Hybrid Transition-Metal Carbides. *J. Phys. Chem. C* **123**, 20664-20674, doi:10.1021/acs.jpcc.9b05962 (2019).
73. M. Han, C. E. Shuck, R. Rakhmanov, D. Parchment, B. Anasori, C. M. Koo, G. Friedman & Y. Gogotsi. Beyond $Ti_3C_2T_x$: MXenes for Electromagnetic Interference Shielding. *ACS Nano.* **14**, 5008–5016 (2020).
74. J. Halim, E. J. Moon, P. Eklund, J. Rosen, M. W. Barsoum & T. Ouisse. Variable range hopping and thermally activated transport in molybdenum-based MXenes. *Phys. Rev. B* **98**, 104202 (2018).
75. J. H. Yang, X. P. Luo, X. M. Zhou, S. Z. Zhang, J. Liu, Y. Xie, L. Lv & L. Chen. Tuning magnetic properties of $Cr_2M_2C_3T_2$ (M = Ti and V) using extensile strain. *Comput. Mater. Sci.* **139**, 313-319, doi:10.1016/j.commatsci.2017.08.016 (2017).
76. Y. Hu, X. Fan, W. Guo, Y. An, Z. Luo & J. Kong. Ordered double-M elements MXenes TiMC: Large in-plane stiffness and ferromagnetism. *Journal of Magnetism and Magnetic Materials* **486**, 165280 (2019).
77. K. Maleski. Solution Processing and Optical Propertiesof 2D Transition Metal Carbides (MXenes) *Drexel University, Philadelphia USA, Ph.D. Desertation* (2020).
78. C. Zhang, B. Anasori, A. Seral-Ascaso, S. H. Park, N. McEvoy, A. Shmeliov, G. S. Duesberg, J. N. Coleman, Y. Gogotsi & V. Nicolosi. Transparent, flexible, and conductive 2D titanium carbide (MXene) films with high volumetric capacitance. *Adv. Mater.* **29**, 1702678 (2017).
79. Z. H. Fu, S. H. Zhang, D. Legut, T. C. Germann, C. Si, S. Y. Du, J. S. Francisco & R. F. Zhang. A synergetic stabilization and strengthening strategy for two-dimensional ordered hybrid transition metal carbides. *Phys. Chem. Chem. Phys.* **20**, 29684-29692, doi:10.1039/c8cp06458j (2018).
80. M. Kurtoglu, M. Naguib, Y. Gogotsi & M. W. Barsoum. First principles study of two-dimensional early transition metal carbides. *MRS Communications* **2**, 133-137, doi:10.1557/mrc.2012.25 (2012).
81. V. N. Borysiuk, V. N. Mochalin & Y. Gogotsi. Molecular dynamic study of the mechanical properties of two-dimensional titanium carbides $Ti_{n+1}C_n$ (MXenes). *Nanotechnology.* **26**, 265705 (2015).
82. G. Plummer, B. Anasori, Y. Gogotsi & G. J. Tucker. Nanoindentation of monolayer $Ti_{n+1}C_nT_x$ MXenes via atomistic simulations: The role of composition and defects on strength. *Comput. Mater. Sci.* **157**, 168-174 (2019).
83. E. Rudy. Ternary phase equilibria in transition metal-boron-carbon-silicon systems. part 5. compendium of phase diagram data. (Aerojet-general corp sacramento ca materials research lab 1969).
84. H. Wang, H. Yuan, S. S. Hong, Y. Li & Y. Cui. Physical and chemical tuning of two-dimensional transition metal dichalcogenides. *Chem. Soc. Rev.* **44**, 2664-2680 (2015).
85. Y. Chen, J. Xi, D. O. Dumcenco, Z. Liu, K. Suenaga, D. Wang, Z. Shuai, Y.-S. Huang & L. Xie. Tunable band gap photoluminescence from atomically thin transition-metal dichalcogenide alloys. *ACS Nano.* **7**, 4610-4616 (2013).
86. M. Ashton, R. G. Hennig, S. R. Broderick, K. Rajan & S. B. Sinnott. Computational discovery of stable M_2AX phases. *Phys. Rev. B* **94**, 054116 (2016).
87. A. S. Ingason, M. Dahlqvist & J. Rosén. Magnetic MAX phases from theory and experiments; a review. *J. Phys.: Condens. Matter* **28**, 433003 (2016).
88. P. Urbankowski, B. Anasori, T. Makaryan, D. Er, S. Kota, P. L. Walsh, M. Zhao, V. B. Shenoy, M. W. Barsoum & Y. Gogotsi. Synthesis of two-dimensional titanium nitride Ti_4N_3 (MXene). *Nanoscale* **8**, 11385-11391 (2016).
89. K. Hantanasirisakul, M. Alhabeb, A. Lipatov, K. Maleski, B. Anasori, P. Salles, C. Ieosakulrat, P. Pakawatpanurut, A. Sinitskii & S. J. May. Effects of Synthesis and Processing on Optoelectronic Properties of Titanium Carbonitride MXene. *Chem. Mater.* **31**, 2941-2951 (2019).
90. X. Liang, Y. Rangom, C. Y. Kwok, Q. Pang & L. F. Nazar. Interwoven MXene Nanosheet/Carbon-Nanotube Composites as Li-S Cathode Hosts. *Adv. Mater.* **29**, 1603040 (2017).
91. X. Tang, X. Guo, W. Wu & G. Wang. 2D Metal Carbides and Nitrides (MXenes) as High-Performance Electrode Materials for Lithium-Based Batteries. *Advanced Energy Materials* **8**, 1801897 (2018).
92. H. Lin, D.-D. Yang, N. Lou, S.-G. Zhu & H.-Z. Li. Functionalized titanium nitride-based MXenes as promising host materials for lithium-sulfur batteries: A first principles study. *Ceram. Int.* **45**, 1588-1594 (2019).
93. M. Li, J. Lu, K. Luo, Y. Li, K. Chang, K. Chen, J. Zhou, J. Rosen, L. Hultman, P. Eklund, P. O. Å. Persson, S. Du, Z. Chai, Z. Huang & Q. Huang. Element replacement approach by reaction with Lewis acidic molten salts to synthesize nanolaminated MAX phases and MXenes. *J. Am. Chem. Soc.* **141**, 4730-4737 (2019).
94. A. Mockuté, J. Lu, E. Moon, M. Yan, B. Anasori, S. May, M. Barsoum & J. Rosén. Solid solubility and magnetism upon Mn incorporation in the bulk ternary carbides Cr_2AlC and Cr_2GaC. *Mater. Res. Lett.* **3**, 16-22 (2015).

Weichen Hong is a doctoral candidate and a research assistant in the Layered Materials and Structures Laboratory in the Department of Mechanical and Energy Engineering at Indiana University–Purdue University Indianapolis. He received his BS and MS degrees in material science engineering from the Wuhan University of Technology, China, in 2017 and 2019, respectively. His research interests include new MAX phases exploration and corresponding MXenes' synthesis, characterization, and applications for energy storage and electronics. Hong can be reached by email at hweichen@purdue.edu.

Brian Cecil Wyatt is a doctoral candidate in the Layered Materials and Structures Laboratory in the Department of Mechanical and Energy Engineering at Indiana University–Purdue University Indianapolis.. He received his BS degree in mechanical engineering from the Rose-Hulman Institute of Technology in 2019. His research includes the mechanical characterization and composition control of two-dimensional nanomaterials as well as the investigation of their interfacial properties in structural composite materials. His current research focuses on the inclusion of MXenes into lightweight metals for bioinspired structural applications. Wyatt can be reached by email at bcwyatt@iu.edu.

Srinivasa Kartik Nemani is a doctoral candidate and a research assistant in the Layered Materials and Structures Laboratory in the Department of Mechanical and Energy Engineering at Indiana University–Purdue University Indianapolis.. He received his MS degree in mechanical engineering from the University of Toledo in 2018. His research interests include MXenes, composites, and hybrids His current research focuses on synthesizing MXenes and developing MXene-reinforced materials for various applications. He has published articles in several journals, including *Advanced Materials Interfaces* and *ACS Applied Materials & Interfaces*. Nemani can be reached by email at snemani@purdue.edu.

Babak Anasori is an assistant professor in the Purdue School of Engineering and Technology at Indiana University–Purdue University Indianapolis.. He received his PhD degree in materials science and engineering from Drexel University in 2014. He is one of the inventors of ordered double-transition metal MXenes, as a result of his postdoctoral research. His current research focuses on the synthesis and characterizations of novel MXenes and their composites. He has co-authored more than 120 journal papers. He co-edited the first book on MXenes in 2019, and he is among the 2019 Global Highly Cited Researchers, recognized by the Web of Science. He is currently the chair of the Early Career Professionals Subcommittee of the Materials Research Society. Anasori can be reached by email at banasori@iupui.edu.